iScience

Article

Ligand preference of EphB2 receptor is selectively regulated by N-glycosylation

Graphical abstract

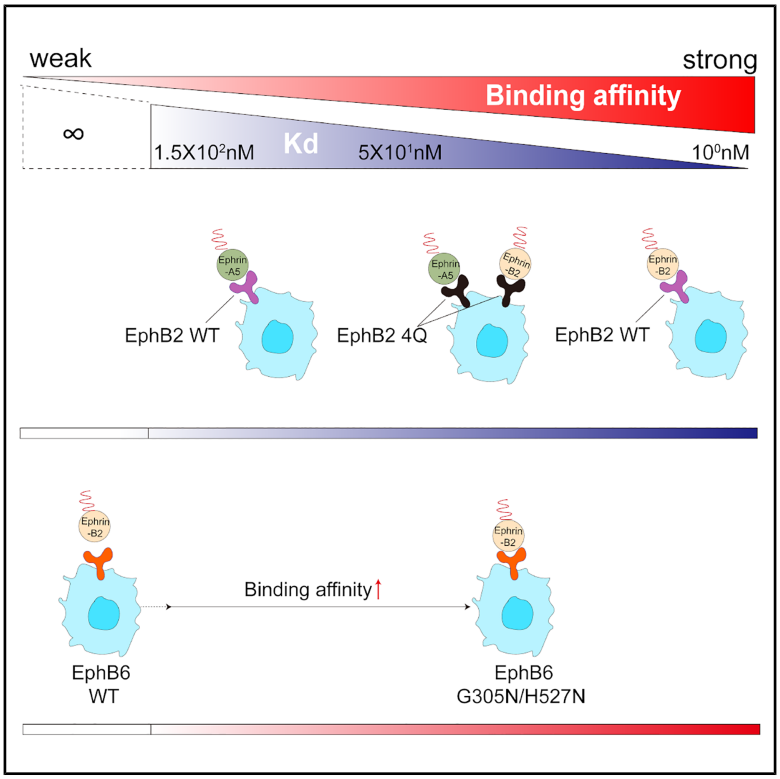

Highlights

- N-glycosylation is important for the binding specificity of EphB2 to ephrin-A5/B2
- Gain-of-function mutation of EphB6 can restore its binding ability to ephrin-B2
- N-glycosylation of EphB2 is required for cell rounding and dendritic spine formation

Authors

Chunyu Lyu, Lin Yuan, Yang Yang, ..., Kang Xiao, Yu Chen, Wei Liu

Correspondence

xiaokang@ustc.edu (K.X.), yu.chen@siat.ac.cn (Y.C.), liuwei@sphmc.org (W.L.)

In brief

Natural sciences; Biological sciences; Biochemistry

Lyu et al., 2025, iScience *28*, 112386
May 16, 2025
https://doi.org/10.1016/j.isci.2025.112386

CellPress

iScience

CellPress
OPEN ACCESS

Article

Ligand preference of EphB2 receptor is selectively regulated by N-glycosylation

Chunyu Lyu,[1,8] Lin Yuan,[3,8] Yang Yang,[1] Dongsheng Zhang,[1] Wei Hu,[4] Keli Zhao,[1] Yuzhen Ding,[1] Wei Chen,[5] Kang Xiao,[1,6,*] Yu Chen,[2,7,*] and Wei Liu[1,9,*]

[1]Shenzhen Key Laboratory for Neuronal Structural Biology, Biomedical Research Institute, Shenzhen Peking University-The Hong Kong University of Science and Technology Medical Center, Shenzhen 518036, China

[2]Chinese Academy of Sciences Key Laboratory of Brain Connectome and Manipulation, Shenzhen Key Laboratory of Translational Research for Brain Diseases, The Brain Cognition and Brain Disease Institute, Shenzhen Institute of Advanced Technology, Chinese Academy of Sciences, Shenzhen–Hong Kong Institute of Brain Science–Shenzhen Fundamental Research Institutions, Shenzhen, Guangdong 518055, China

[3]Guangdong Provincial Key Laboratory of Brain Science, Disease and Drug Development, HKUST Shenzhen Research Institute, Shenzhen, Guangdong 518057, China

[4]The First Affiliated Hospital, Zhejiang University School of Medicine, Hangzhou 310003, Zhejiang, China

[5]Department of Cell Biology, Zhejiang University School of Medicine, and Liangzhu Laboratory, Zhejiang University, Hangzhou 310000, Zhejiang, China

[6]HKUST Shenzhen-Hong Kong Collaborative Innovation Research Institute, Futian, Shenzhen 518045, China

[7]SIAT-HKUST Joint Laboratory for Brain Science, Chinese Academy of Sciences, Shenzhen 518055, China

[8]These authors contributed equally

[9]Lead contact

*Correspondence: xiaokang@ustc.edu (K.X.), yu.chen@siat.ac.cn (Y.C.), liuwei@sphmc.org (W.L.)

https://doi.org/10.1016/j.isci.2025.112386

SUMMARY

The Eph receptors and their ephrin ligands play important roles in cell communication and neuron development. Eph interacts with ephrin in a complex manner. Here, we found ephrin-B2 instead of well-recorded ephrin-A5 specifically recognize and activate EphB2 receptor in primary cortical neurons. Domain-swapping and N/Q mutagenesis results show that the ectodomain of EphB2 and its N-glycosylation sites are critical for the ephrin binding selectivity. The N265, N336, N428, and N482Q mutant EphB2 cannot distinguish ephrin-B2 from ephrin-A5. Furthermore, the N-glycosylation sites in EphB2 are evolutionarily conserved and the N-glycan-directed binding strategy is commonly used in other Eph family members. A gain-of-function EphB6 mutant restores its ephrin-B2 binding ability. Finally, EphB2 is robustly glycosylated in the mouse brain and N-glycosylation is required for EphB2 signaling-induced cell rounding and dendritic spine formation. Collectively, our findings provide a molecular basis to understand the exquisite Eph/ephrin interaction preferences.

INTRODUCTION

The erythropoietin-producing hepatocellular (Eph) receptors, comprising the largest family of receptor tyrosine kinases (RTKs), enable bidirectional communication with ephrin ligands.[1] Their interaction initiates both "forward" signaling pathways that induce receptor clustering and autophosphorylation and "reverse" signaling pathways that trigger phosphorylation and downstream signaling cascades of the ephrin ligands.[1–5] In mammals, Eph family receptors are classified into the A-subclass and B-subclass based on sequence similarity and their preference for binding a particular subclass of ephrin.[6] The Eph receptors and ephrin ligands constitute a vital signaling system governing various physiological functions, including tissue-boundary formation, angiogenesis, axon guidance, and nervous system development.[7–10] Dysregulation of this system is implicated in numerous pathological conditions, such as cancer and neurological disorders, making the Eph/ephrin signaling axis a promising therapeutic target.[11–14]

Previous biochemical studies suggest that there is a promiscuous interaction rule between ephrin and Eph, which could partially account for the functional redundancy of Eph.[10,15–17] For example, EphA2 was shown to interact with not only ephrin-As but also ephrin-B2.[14] However, it is still unknown how specific signaling outcomes are achieved via Eph/ephrin promiscuous interactions, considering multiple Eph/ephrin pairs expressed within one tissue in overlapping expression patterns.[7,9,18] And the source of promiscuity remains unclear.

In this study, we found that ephrin-B2 can specifically recognize and activate the EphB2 receptor in primary cultured

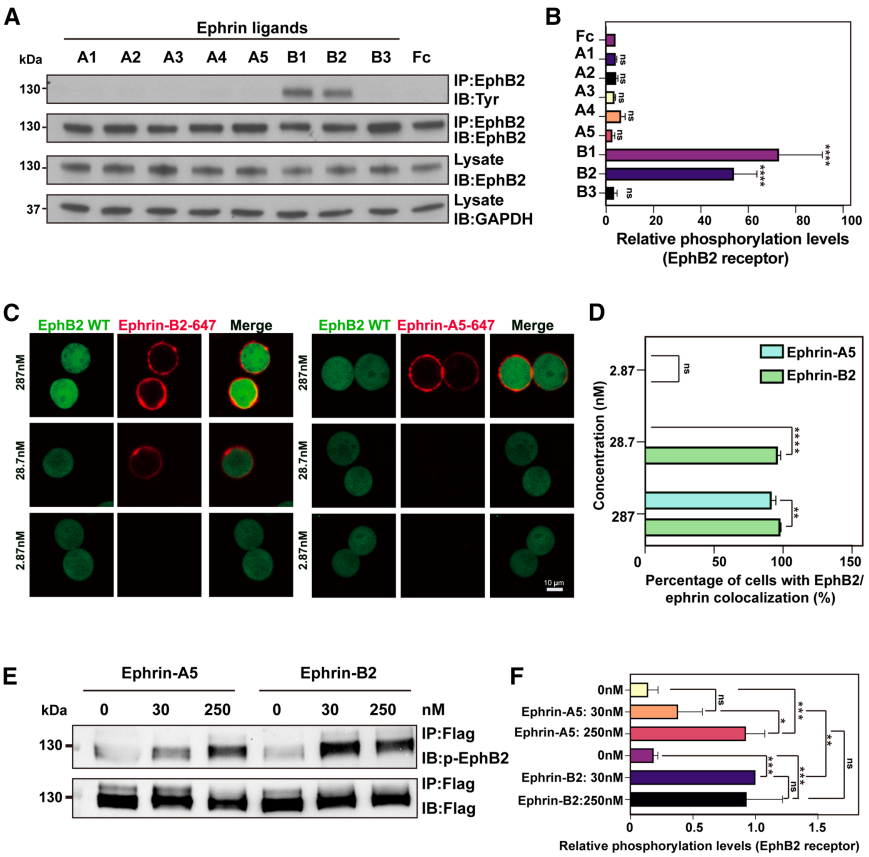

Figure 1. The ephrin-A5 and ephrin-B2 ligands exhibit distinct activation capacities to the EphB2 receptor

(A) Representative images from western blot analysis of endogenous EphB2 following immunoprecipitation from rat cortical neurons, GAPDH served as a loading control.

(B) Relative EphB2 phosphorylation level after treatment with Fc or Fc-ephrin correlated to (A). Statistical significance was performed by one-way ANOVA with Dunnett's post hoc test; ns, not significant; $^{****}p < 0.0001$ compared to Fc.

(C and D) Representative confocal microscopy images of ligand-stimulated EphB2/ephrins colocalization. Green represents cells expressing EphB2 and red is 647 labeled pre-clustered ephrin-A5 or ephrin-B2. Scale bar: 10 μm. The averaged ratios of cells exhibiting EphB2/ephrins colocalization post-stimulation are plotted as (D). Statistical significance was performed by two-way ANOVA; Tukey's post-hoc multiple comparisons test; ns, not significant; $^{**}p < 0.01$, $^{****}p < 0.0001$; $n = 3$, from at least 3 independent experiments with over 50 cells per panel.

(E) Representative western blot results of immunoprecipitated C-terminal 3 × FLAG EphB2 in HEK293T cells after treatment with pre-clustered ephrin-A5 or ephrin-B2 for 1 h.

(F) Relative amount phospho-EphB2 from (E), one-way ANOVA; Tukey's post-hoc multiple comparisons test, ns, not significant; $^{*}p < 0.05$; $^{**}p < 0.01$, $^{***}p < 0.001$; ($n = 3$).

All data are presented as mean ± SD.

cortical neurons, while ephrin-A5 cannot. Therefore, the ligand-binding specificities of EphB2 toward these two well-known ligands, ephrin-A5 and ephrin-B2, were extensively investigated by biochemical and cell-based assays. Our results unraveled that EphB2 discriminated ephrin-A5 and ephrin-B2 ligands with significantly different affinities (a difference of two orders of magnitude), while disruption of N-glycosylation diminished this binding preference. Specifically, the N265, N336Q mutant enhanced the specific binding to ephrin-A5, while the N428, N482Q mutant decreased the interaction with ephrin-B2. The non-glycosylated EphB2 ectodomain diminished the binding specificity to ephrin-A5/B2. N-glycosylation deficient mutation in the EphB2 ectodomain impaired the receptor's ability to specifically recognize ephrin-A5/B2 ligands. Furthermore, sequence alignment analysis showed that these N-glycosylation sites are evolutionarily conserved in EphB2 and N-glycosylation commonly exists in other Eph family members, indicating that N-glycosylation may serve as an evolutionarily important and general regulator for Eph receptors. Notably, the gain-of-function mutations of EphB6 can restore specific recognition ability to ephrin-B2. Finally, disruption of N-glycosylation sites impaired the functions of EphB2 in cell rounding and dendritic spine formation. In summary, our findings reveal that N-glycosylation could be a general regulatory mechanism of the Eph family.

RESULTS

Ephrin-A5 and ephrin-B2 ligands show different EphB2 activation capacities

To explore EphB2 activation and signaling *in vivo*, primary cortical neurons were cultured for 10 days *in vitro* (DIV10). Subsequently, the cells were stimulated with 2 μg/mL (~100 nM) of various pre-clustered Fc-ephrin ligands for 1 h, and EphB2 receptor activation was assessed via immunoprecipitation by EphB2 antibody, followed by western blotting with an anti-phosphotyrosine antibody. Remarkably, ephrin-B2 specifically activated the EphB2 receptor compared to the Fc control and ephrin-A5 (Figures 1A and 1B). Similar specific interaction was also observed between EphA4 and ephrins (Figures S1A and S1B).

In addition, to investigate the ligand preference of EphB2, we monitored the ligand-induced ligand/receptor colocalization in cultured Expi293F cells, referencing to the study of *Scott E. Fraser* et al.[19] To achieve pre-clustering of ephrin proteins, Streptavidin-labeled 647 dye was employed to bind with purified biotinylated ephrin proteins. These streptavidin-mediated clustered ephrin proteins are referred to as pre-clustered ephrin ligands later. The pre-clustered ephrin proteins were then used to stimulate Expi293F cells over-expressing EphB2. At a concentration of 28.7 nM, pre-clustered ephrin-B2 ligand significantly induced EphB2/ephrin-B2 colocalization on the cell

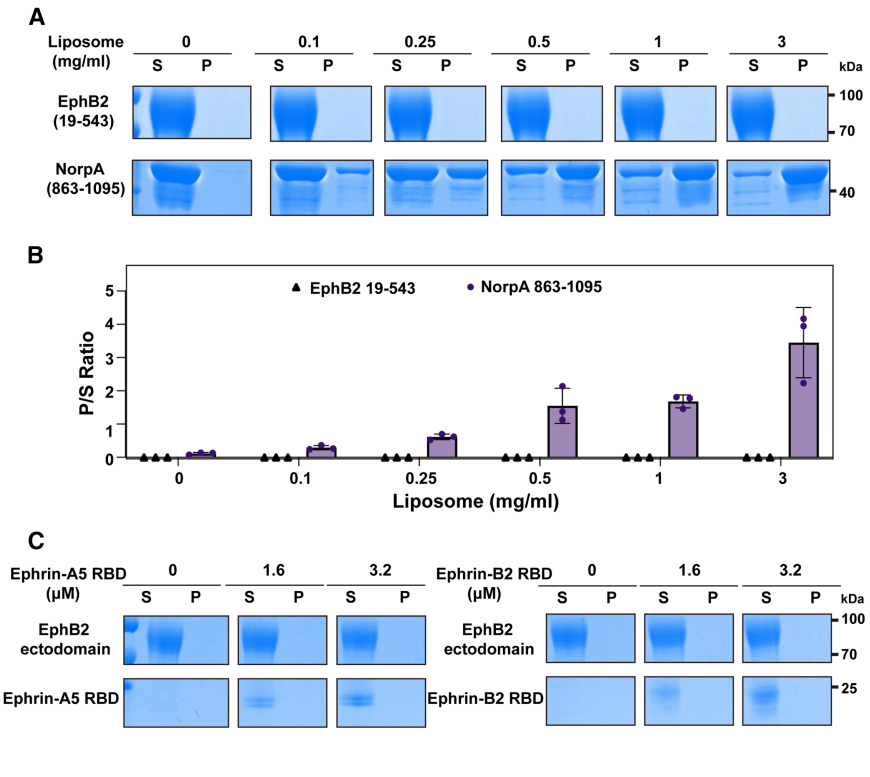

Figure 2. EphB2 cannot bind to liposomes with/without ephrin-A5/B2

(A) A dose-dependent assay detecting the liposome binding of EphB2 (residues 19–543), with NorpA (residues 863–1095) serving as a positive control. S and P denote proteins recovered in the supernatants and pellets, respectively, in the centrifugation-based liposome binding assays.

(B) Quantification of protein percentage in the pellet fraction was calculated from three independent experiments.

(C) A dose-dependent assay detecting the liposome binding of EphB2 (residues 19–543) with different concentrations of pre-clustered ephrin-A5 or ephrin-B2. The concentration of liposomes is 1 mg/mL. The experiment was independently repeated three times.

All data are presented as mean ± SD.

membrane surface ($p < 0.0001$). In a higher concentration (287 nM), the specific activation disappeared, and both pre-clustered ephrin-A5 and ephrin-B2 induced the EphB2/ephrins colocalization (Figures 1C and 1D). Therefore, 28.7 nM is a threshold ephrin concentration defining the binding preference of EphB2 for ephrin-A5 and ephrin-B2 in the Expi293F cell system.

Then, the ligand preference of EphB2 was further assayed by ligand-induced autophosphorylation of EphB2. EphB2-expressing Expi293F cells were stimulated with pre-clustered ephrin proteins at varying concentrations (0, 30, and 250 nM). Western blotting analysis was used to monitor the levels of EphB2 activation by measuring the phosphorylation of a specific tyrosine in the juxtamembrane region ($pY^{594/604}$). Results showed significant difference in EphB2 phosphorylation induced by ephrin-A5 and ephrin-B2 at 30 nM, while there was no statistical difference at 250 nM (Figures 1E and 1F). These findings were well aligned with the aforementioned ligand-induced ligand/receptor colocalization results.

Lipid binding property is not responsible for ligand preference of EphB2

To investigate which domains of EphB2 are responsible for the specific binding of ephrin-B2, extracellular and intracellular parts of EphB2 were swapped with those of EphA4 respectively to observe the colocalization behaviors at the cell membrane (Figure S2A). As a control, the full-length wild-type EphB2 (EphB2 WT) receptor displayed ligand-induced colocalization, whereas the EphA4 receptor did not. Only the chimeric EphB2 containing the ectodomain of EphB2 can respond to ephrin-B2 (287 nM) (Figures S2B and S2C), suggesting that the ectodomain of EphB2 is responsible for the specific ephrin-B2 ligand binding.

Previous studies have shown that the ectodomain of membrane proteins can interact with lipids, thus affecting the dynamic behavior of the receptor at the cell surface.[20,21] Notably, the membrane-proximal fibronectin domain 2 within the ectodomain of EphA2 can bind to lipids, which alters receptor orientation and thus affects accessibility to the ephrin ligands.[22] Based on these findings, we investigated whether the ectodomain of EphB2 could similarly interact with the membrane, thereby influencing its selective binding to different ligands. We purified the EphB2 extracellular domain (residues 19–543) through the His-tag affinity purification column followed by Superdex-200 size-exclusion chromatography and examined its binding to liposomes. Neither EphB2 alone nor its complex with ephrin-A5 or ephrin-B2 showed significant interactions with liposomes (Figures 2A–2C), ruling out the potential role of lipid binding in ligand preference of EphB2.

Non-glycosylated EphB2 ectodomain diminishes the binding specificity to ephrin-A5/B2

Besides membrane binding properties, glycosylation of the protein is also important for the behavior of RTKs.[21,23–25] This post-translational modification can influence protein conformation and ligand-receptor interactions.[24,26–29] Therefore, potential glycosylation sites on mouse EphB2 were predicted at positions N265, 336, 428, and 482 using the NetNGlyc 1.0 Server. Subsequently, after endoglycosidase PNGase F treatment, the purified EphB2 ectodomain displayed a significant reduction in molecular mass compared to untreated-EphB2 (Figure 3A, top), indicating the presence of N-glycosylation. Besides, in the crystal structure of extracellular domain of EphB2, four N-glycosylation sites are identified: Asn265, Asn336, Asn428, and Asn482.[30] These four N-glycosylation sites were further confirmed and characterized by the mass spectrometry analysis (Figure S3). Similarly, EphB2 from hippocampus tissues of 10-day-old and adult mice also showed a reduction in molecular weight from approximately

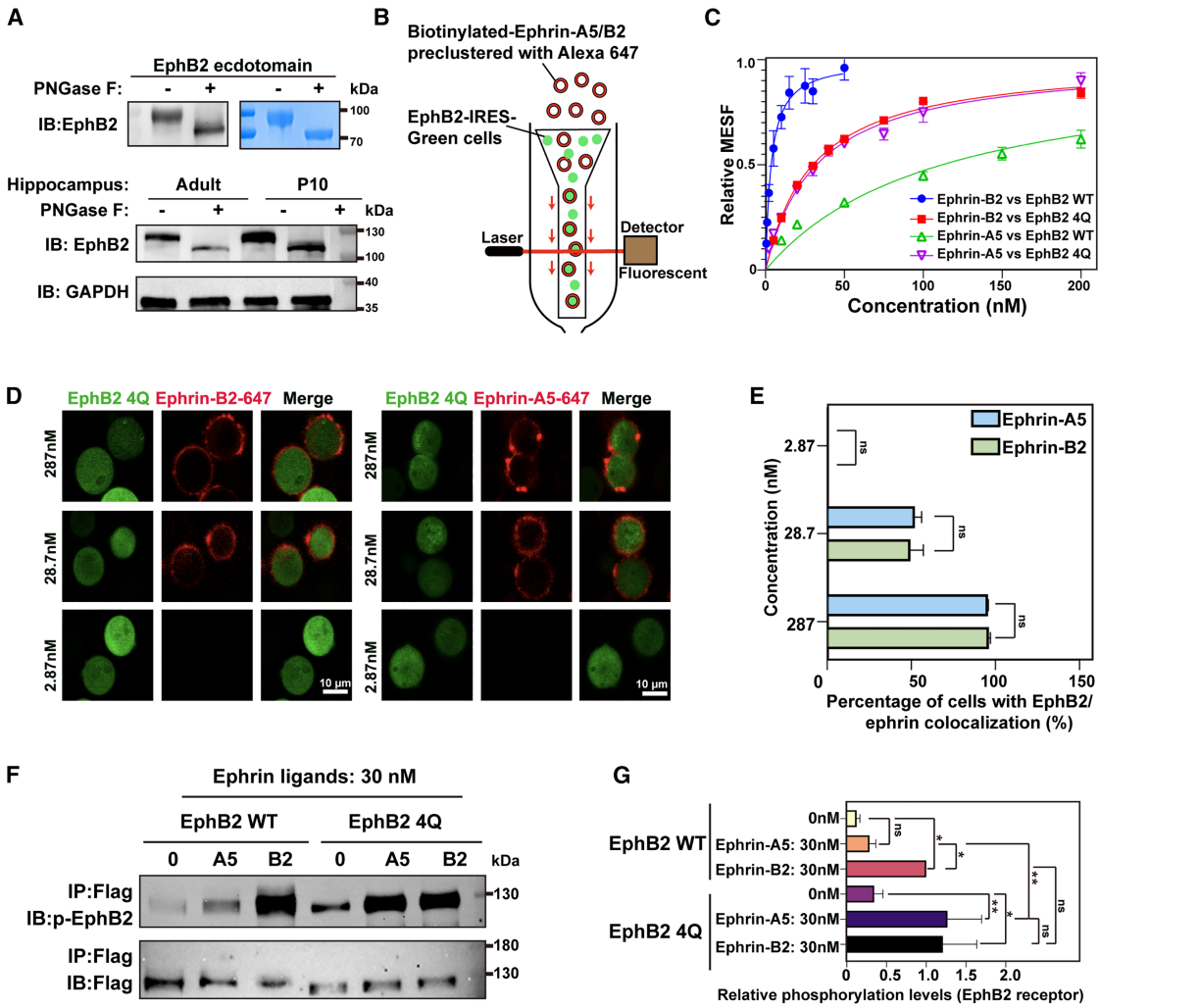

Figure 3. The glycosylation of EphB2 is indispensable for ephrin-A5/B2 binding specificity

(A) Top: western blot and Coomassie brilliant blue staining results of purified EphB2 protein before/after PNGase F treatment. Bottom: western blot results of endogenous EphB2 from adult and P10 mice hippocampus before/after PNGase F enzyme treatment. GAPDH served as a loading control.

(B) Flow diagram of FCM assay. EphB2-expressing cells bound by pre-clustered ephrin-A5 or ephrin-B2 were recorded by flow cytometry and translated to the relative MESF values.

(C) The FCM results are analyzed by the "one-site specific binding" model to fit the saturation binding curves and obtain the K_D values. The K_D of EphB2 WT to ephrin-B2 and ephrin-A5 are 3.526 nM and 111.9 nM; the K_D of EphB2 4Q to ephrin-B2 and ephrin-A5 are 29.91 nM and 32.29 nM.

(D and E) Representative confocal microscopy images of ligand-induced ligand/receptor colocalization assays upon stimulating with ephrin ligands. Green represents cells expressing EphB2 4Q, and red represents 647-labeled pre-clustered ephrin ligands. Scale bar: 10 μm. Averaged ratios of cells with EphB2 4Q/ephrins colocalization after stimulation are plotted as (E). Statistical significance was performed by two-way ANOVA; Tukey's post-hoc multiple comparisons test; ns, not significant; (n = 3).

(F) Representative western blot results of immunoprecipitated C-terminal 3 × FLAG EphB2 WT or EphB2 4Q in HEK293T cells after ephrin-A5 or ephrin-B2 stimulation.

(G) Measurement of relative EphB2 tyrosine phosphorylation, correlated with (F). Statistical significance was performed by one-way ANOVA; Tukey's post-hoc multiple comparisons test, ns, not significant; *$p < 0.05$; **$p < 0.01$; (n = 3).

All data are represented as mean ± SD.

130–117 kDa (the calculative molecular weight of EphB2) after PNGase F treatment (Figure 3A, bottom). These findings demonstrated that N-glycosylation does exist in both the purified protein and brain tissue.

Next, to quantitatively measure the binding affinities of Eph/ephrin interactions in a membrane environment, full-length EphB2 was expressed on the surface of Expi293F cells. Flow cytometry (FCM) was utilized to investigate the impact of glycosylation on EphB2's binding specificity on the surface of cells (Figure 3B). As a control, endogenous expression of EphB2 in Expi293F cells was excluded (Figure S4A). Full-length EphB2 was expressed on the Expi293F cell membranes through

transient lentivirus infection (Figure S4B), with co-expressed GFP protein serving as an indicator of EphB2 expression (Figure S4C). By recording the mean fluorescence intensity (MFI) values of cells expressing either EphB2 WT or EphB2 4Q (N-glycosylation sites to glutamine [Q] to generate N-glycosylation deficient EphB2: N265, N336, N428, and N482Q) in response to different concentrations of pre-clustered ligands, the MFI values were converted into molecules of equivalent soluble fluorochrome (MESF), to generate saturation binding curves for deriving the dissociation constant (K_D) values (Figure S4D). Time-dependent binding experiments were performed to determine the reaction time between EphB2 and ephrin-A5/B2 in Figure S4E. As a control, the nonspecific interaction between GFP-expressing cells and ephrin-A5/B2 was not detected (Figure S4F). Analysis of the binding curve using a one-site specific binding model revealed that the K_D value of ephrin-A5 interacting with cells expressing EphB2 WT (K_D = 111.9 nM) was much weaker than ephrin-B2 (K_D = 3.526 nM). Interestingly, EphB2 4Q mutant eliminated the difference in K_D values between ephrin-A5 (K_D = 32.29 nM) and ephrinB2 (K_D = 29.91 nM) treated groups (Figure 3C). Similarly, ephrin-B1 (K_D = 6.642 nM), another major signaling partner for EphB2, behaved like ephrin-B2 but not ephrin-A5 (Figure S4G). The relatively weak binding of EphA4/ephrin-B2 (K_D = 500.9 nM) further supported the findings of domain-swapping results and the activation of endogenous EphA4 by ephrins in cortical neurons (Figures S1, S2, and S4H). In addition, EphB2 4Q-expressing cells can be colocalized by ephrin-A5 at a concentration of 28.7 nM (Figures 3D and 3E). This result was further confirmed by immunoprecipitation experiments that EphB2 4Q-expressing cells can equally be activated by ephrin-A5 and ephrin-B2 (Figures 3F and 3G). These findings suggest that the glycosylation deficient mutant abolished the binding selectivity of EphB2 toward different ligands.

Different glycosylation sites of EphB2 ectodomain play distinct roles

To investigate the mechanism of how defective glycosylation can abolish the binding selectivity of EphB2 toward different ligands, we performed a comprehensive mutagenesis study of glycosylation sites (Figures 4A and S5A; Table S1). The ephrin-A5 and ephrin-B2 ligand binding capacities to EphB2 glycosylation deficient mutants were systematically examined. The N265, N336Q double mutant significantly increased the binding affinity to ephrin-A5 (K_D = 31.37 nM), resembling the affinity of EphB2 4Q mutant (K_D = 32.29 nM). In contrast, the N428, N482Q double mutant significantly weakened the binding with ephrin-B2 ligand (K_D = 12.27 nM). The N265, N336Q double mutant had minimal effect on the binding affinity with ephrin-B2 ligand (K_D = 7.015 nM) compared with EphB2 WT (K_D = 3.526 nM). While the N428, N482Q double mutant almost did not affect the interaction between EphB2 and ephrin-A5 (K_D = 120.3 nM). Further mapping results showed that the single mutant had a marginal effect compared to the double mutant (Figures 4B and S5B–S5G).

Furthermore, to evaluate the impact of the aforementioned mutations, ligand-induced ligand/receptor colocalization assays were conducted. The N265, N336Q mutation increased the EphB2/ephrin-A5 colocalization by ephrin-A5 (28.7 nM), resembling EphB2 4Q mutation. The N428, N482Q mutation decreased the EphB2's colocalization by ephrin-B2 (28.7 nM) (Figures 4C and 4D). The ability of ligand-induced single mutant colocalization is similar to double mutant (Figure S5H). Ligand-induced autophosphorylation of EphB2 was also examined. Consistently, the N265, N336Q mutation can increase the sensitivity of EphB2 in terms of kinase activity by ephrin-A5 compared with EphB2 WT. The N428, N482Q mutation attenuated the activation of EphB2 induced by ephrin-B2. Ephirn-A5 and ephrin-B2 ligands exhibited similar potency to activate the EphB2 4Q mutant (Figures 4E and 4F). Taken together, different N-glycosylation sites within EphB2 ectodomain play distinct roles in ligand selectivity.

Glycosylation is a potential common regulation mechanism in the Eph family

To explore the potential evolutionary role of distinct N-glycosylation sites in regulating EphB2 receptor's binding specificity, we first conducted a sequence alignment analysis of EphB2 from zebrafish to human. The N-glycosylation sites are highly conserved during evolution (Figure 5A), indicating that N-glycosylation may play a significant role in EphB2's function. Interestingly, N-glycosylation sites also exist in other Eph family members (Figures 5B and S6). In EphB6, there is only one N-glycosylation site, lacking the critical N-glycosylation sites for ephrin-B2 binding found in EphB2. After ^{305}GDK^{307}-to-^{305}NDS^{307} and ^{527}HSF^{529}-to-^{527}NSS^{529} mutations were introduced at the sites corresponding to Asn265 or Asn482 of EphB2, EphB6 gained the binding ability to ephrin-B2 (K_D = 20.94 nM) compared to the wild-type (Figures 5C and 5D), suggesting a general regulatory role of N-glycosylation in determining ligand preferences among EphB family members. More importantly, we surveyed the COSMIC (Catologue of Somatic Mutations In Cancer) cancer somatic mutation database (http://cancer.sanger.ac.uk/cosmic; a collection of somatic mutations found in cancer patients mainly from large-scale genome sequencing studies),[31] and found that numerous N-glycosylation deficient mutations occur in almost every subtype of Eph genes except for EphA2, EphA10 and EphB3 (Figure 5E).

N-glycosylation is functionally required for cell rounding and dendritic spine morphogenesis

EphB2 is crucial for neuronal morphogenesis and cell retraction during neurodevelopment, and the application of soluble active forms of ephrin ligands typically promotes spine formation and maturation or induces cell rounding.[32–34] The cell retraction assay was first used to investigate whether N-glycosylation is involved in cellular responses mediated by Eph/ephrin interactions. To minimize potential *trans*-signaling from neighboring cells, all experiments were performed in low-density cultures (at about 30% confluency or below).[35] Cells were infected with lentivirus expressing EphB2 WT, EphB2 4Q, or a GFP control. Consistent with previous reports, in the EphB2 WT group, pre-clustered ephrin-B2 significantly induced cell rounding, while ephrin-A5 exhibited subtle effects (Figures 6A, top and 6B). In contrast, GFP control cells did not respond to either pre-clustered ephrin ligand (Figures 6A, bottom and 6B). Interestingly, in the EphB2 4Q group, there was no difference between

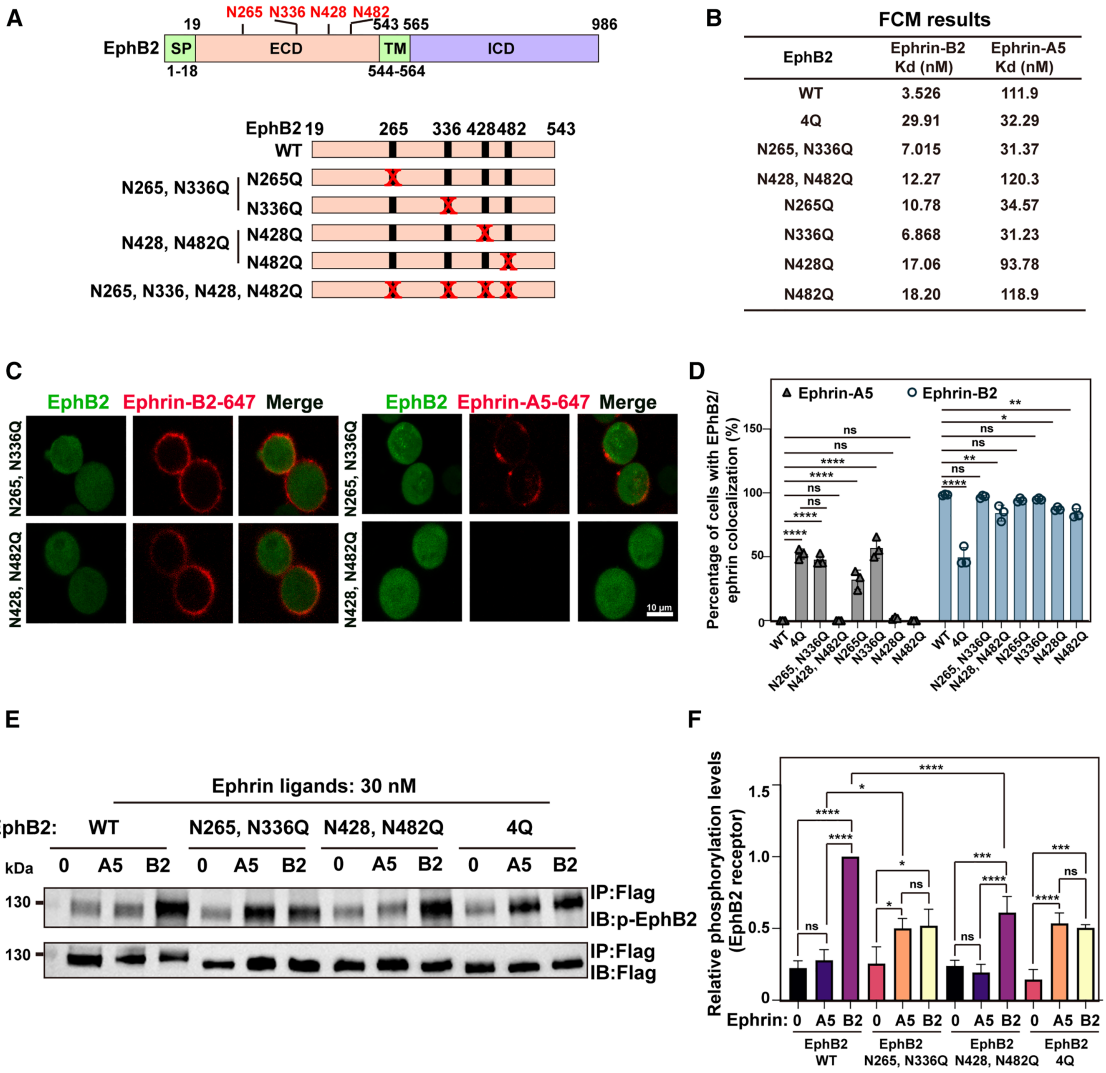

Figure 4. Mapping the critical N-glycosylation sites involved in the ligand preference of EphB2

(A) Schematic diagram of EphB2 protein. Full-length EphB2 was separated into extracellular domain (ECD) and intracellular domain (ICD). SP, signal peptide; TM, transmembrane domain. Schematic of various EphB2 N-Q (asparagine to glutamine) mutations used in this study.

(B) Summary of FCM-derived binding affinities (K_D) of EphB2 to ephrin-A5/B2 with different mutations.

(C) EphB2/ephrins colocalization assays of EphB2 N265, N336Q-expressing, and N428, N482Q-expressing cells upon stimulating with ephrin-A5 or ephrin-B2 ligands. Scale bar: 10 μm.

(D) Summary plot of EphB2/ephrins colocalization: averaged ratios of cells with EphB2 WT and different N-glycosylation mutants in ligand-induced ligand/receptor colocalization, subjected to two-way ANOVA; Tukey's post-hoc multiple comparisons test; ns, not significant; $^{*}p < 0.05$; $^{**}p < 0.01$, $^{****}p < 0.0001$; ($n = 3$).

(E) Representative western blot results of immunoprecipitated c-terminal 3 × FLAG EphB2 WT, EphB2 N265, N336Q, EphB2 N428, N482Q, and EphB2 4Q in HEK293T cells after ligands stimulation.

(F) Measurement of relative EphB2 tyrosine phosphorylation, correlated with (E). Statistical significance was performed by one-way ANOVA; Tukey's post-hoc multiple comparisons test, ns, not significant; $^{*}p < 0.05$; $^{***}p < 0.001$, $^{****}p < 0.0001$; ($n = 3$).

All data are represented as mean ± SD.

ephrin-A5 and ephrin-B2 treatments (Figures 6A, middle and 6B). A control blot was conducted to affirm that expression level of EphB2 4Q mutant is similar to that of EphB2 WT (Figures 6C and 6D).

The cortical neurons showed robust N-glycosylation of EphB2 during the development (Figures 7A and 7B). To test the roles of N-glycosylation of EphB2 in synapse formation, we overexpressed EphB2 WT, EphB2 4Q, or a GFP control in primary rat hippocampal neurons on DIV11. Neuronal morphogenesis was examined on DIV14, a critical time point for EphB2 synapse maturation function.[10] EphB2 WT overexpression did not significantly affect dendritic arborization, although it increased the number of dendritic spines compared with the GFP control (Figures 7C–7E). However, the number of dendritic protrusions

A

EphB2	N265	N336	N428	N482
Human	263 VENGTVCR 270	332 ISSVNETS 339	426 SVNITTNQ 433	478 SEYNATAI 486
Macaque	263 VENGTVCR 270	332 ISSVNETS 339	426 SVNITTNQ 433	478 SEYNATAI 486
Mouse	263 VENGTVCR 270	332 ISSVNETS 339	426 SVNITTNQ 433	478 SEYNATAI 486
Rat	263 VENGTVCR 270	332 ISSVNETS 339	426 SVNITTNQ 433	478 SEYNATAI 486
Chicken	263 VENGTVCR 270	332 ISSVNETS 339	426 SVNITTNQ 433	479 SELNSTAV 487
Zebrafish	266 VENGTVCR 273	335 ISSVNETS 342	428 SVNITTNQ 435	482 TEHNSSMV 489

B

EphB2	N265	N336	N428	N482
mEphB1	262 ENSVACKA 269	332 IVNETSII 339	424 SVNITTNQ 431	477 EFNSSMAR 484
mEphB2	263 VENGTVCR 270	332 SVNETSLM 339	426 SVNITTNQ 433	478 EYNATAIK 486
mEphB3	269 AAKESQCR 276	341 NVNETSLI 348	437 AVNITTNQ 444	489 KGIASTVT 496
mEphB4	262 AESNKVCR 269	333 HLNGSTLR 340	424 PVNVTTDR 431	478 PSSVRFLK 486
mEphB6	303 ARGDKLCQ 310	374 EVQGSALM 381	471 AINVSTSH 478	525 ESHSFTMT 532

C

EphB Receptor	Ephrin-B2 Kd (nM)	R square
EphB2 WT	3.558	0.9676
EphB3 WT	33.76	0.9494
EphB4 WT	15.30	0.9570
EphB6 WT	nd	0.9787
EphB6 NSS^{527}	50.89	0.9681
EphB6 NDS^{305}/NSS^{527}	20.94	0.9503

D

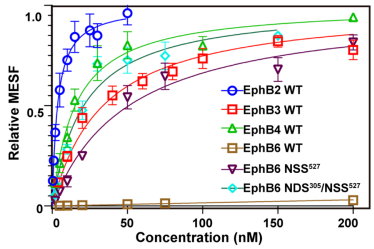

E

N-glycosylation deficient mutations			
Eph	NXT/S	NXT/S	Cancer type
A1	N414S		Prostate carcinoma
A3	N232K		Large intestine
	N337K N404K		Lung adenocarcinoma
	N391I		Chondrosarcoma
A4	N408H		Haematopoietic neoplasm
A5	N264K	S266Y/F/C	Lung/Malignant melanoma/
		T302N	Squamous cell carcinoma
		S425F	/Haematopoietic neoplasm
A6		S399Y/F	Endometrioid carcinoma /Malignant melanoma
A7		T345I	Large intestine carcinoma

N-glycosylation deficient mutations			
Eph	NXT/S	NXT/S	Cancer type
A8		T434I	Hepatocellular carcinoma
B1		T336M	Intestinal adenocarcinoma
	N426S		Lung carcinoma
	N480S	S482F	Basal cell carcinoma
B2	N265D		Clear cell carcinoma of kidney
B4	N335D		Lung adenocarcinoma
	N426S		Stomach adenocarcinoma
B6	N481S	S483I	Mesothelioma/Liver carcinoma

Figure 5. Ectodomain N-glycosylation is evolutionarily conserved in EphB2 and plays important roles in other EphB family members

(A) Multiple sequence alignment analysis of EphB2 from zebrafish to human. N-glycosylation sites are highlighted in red.

(B) Sequence alignment analysis of EphB receptors.

(C and D) Summary of FCM-derived K_D between ephrin-B2 ligand and different EphB receptors (C), along with the corresponding saturation binding curves (D).

(E) Summary of N-glycosylation deficient mutations of Eph receptors identified in cancer patients.

was dramatically reduced in neurons overexpressing EphB2 4Q (Figure 7E). These results suggest that N-glycosylation is functionally required for dendritic spine morphogenesis in cultured hippocampal neurons.

DISCUSSION

Increasing evidence indicates that N-glycosylation is an important post-translational regulator of RTK.[23–26,36,37] In this study, we discovered that distinct activation of EphB2 by ephrin-A5 and ephrin-B2 relied on N-glycosylation of the ectodomain. Glycosylation deficient mutant diminished ligand selectivity of EphB2 and led to downstream changes in cell behavior. Interestingly, N-glycosylation is not only evolutionarily conserved in EphB2 but also commonly exists in other Eph family members. Re-introducing the N-glycosylation site recovers the interaction between EphB6 and ephrin-B2, providing the possibility to manipulate the Eph/ephrin selectivity at the post-translational level. More importantly, robust N-glycosylation of EphB2 indeed exists in brain tissue and is essential for spine morphogenesis in cultured neurons. Thus, this study discovered and provided a molecular basis to manipulate Eph/ephrin interactions by N-glycosylation.

Prior studies systematically examined the apparent binding affinities of Eph/ephrin interactions, suggesting that the binding of ephrin to Eph is promiscuous, which could partially explain their redundant functions.[15,16] However, these methods did not provide the membrane environment required for Eph/ephrin interactions. Hence, we developed a cell-based method to quantify the binding specificities of Eph/ephrin interactions.[38,39] Specifically, this method offers three advantages as follows. (1) FCM avoids safety issues compared to the classical radioactive ligand labeling method.[39–41] Although FCM has relatively lower sensitivity, it can still accurately measure high-affinity ligand-receptor interactions at nanomolar levels.[38,39] (2) Besides, non-cell-based ELISA, SPR (Surface Plasmon Resonance), and NMR (Nuclear Magnetic Resonance) methods examine binding affinities between Eph receptors and ephrin ligands in solution.[15,16,42,43] In contrast, FCM replicates natural binding conditions of full-length receptors, preserving proper protein folding in membrane environments, posttranslational modifications and not needing to express and purify the target receptors.[44–46] (3) In addition, FCM has multiple laser channels, providing possibilities to label different ligands simultaneously, which allows for exploring the competitive interactions between one receptor and different ligands at same time. Thus, FCM can be a useful tool for further studies of other specific Eph/ephrin interactions.

Our FCM analysis showed that the K_D of membrane-bound EphA4 receptors with pre-clustered ephrin-B2 was measured to be approximately 500 nM (Figure S4H). Consistently, 100 nM of ephrin-B2 nearly could not activate endogenous EphA4 in cultured cortical neurons (Figure S1), and 287 nM of ephrin-B2 was not able to induce significant EphA4/ephrin-B2 colocalization (Figure S2). Moreover, high concentration of

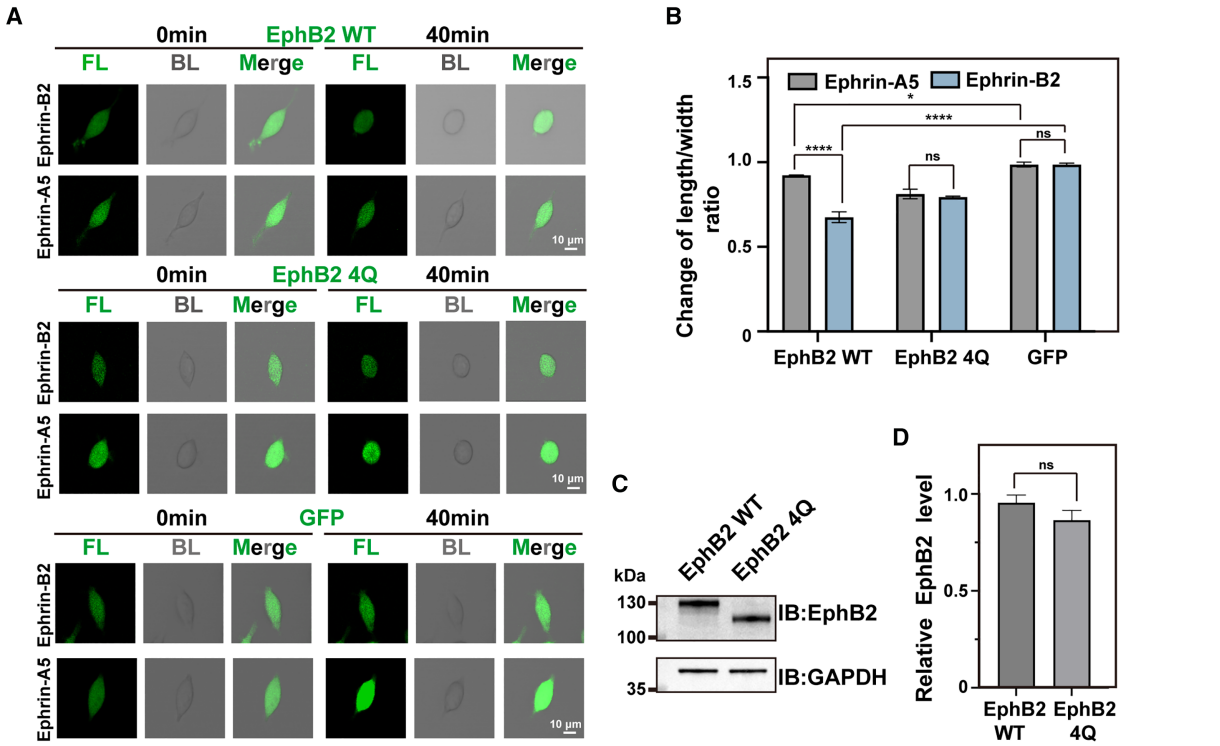

Figure 6. Impacts of the N-glycosylation on EphB2's function in cell contraction in HEK293T cells

(A) HEK293T cell contraction responses after 40 min treatment of pre-clustered ephrin-A5/B2 (each 250 nM). HEK293T were transiently infected with EphB2 WT, EphB2 4Q, or a GFP control lentivirus. Scale bar: 10 μm.

(B) Plotted are the mean length-to-width ratios of adherent cells before and after stimulation. Statistical significance was determined using two-way ANOVA; Tukey's post-hoc multiple comparisons test, ns, not significant, $^{*}p < 0.05$ and $^{****}p < 0.0001$; ($n = 3$, with 10 cells imaged per panel).

(C) Representative western blotting image of EphB2 protein from HEK293T cells infected with EphB2 WT or 4Q lentivirus. GAPDH was used as a loading control.

(D) Relative EphB2 expression level of (C). The relative EphB2 expression level is represented by the ratio of EphB2/GAPDH. Statistical analysis was performed by unpaired t test, ns, not significant.

All data are represented as mean ± SD.

ephrin-B2 (~400 nM) can activate EphA4 signaling in endothelial cells.[47]

In contrast, ephrin-B2 is a well-known ligand of the EphA4 receptor. Gale et al. found that the K_D of pre-clustered EphA4-Fc with membrane-bound ephrin-B2 was 8.60 nM by ELISA.[48,49] The major difference is: they used soluble receptor to stimulate membrane-bound ligand, while we used soluble ligand to stimulate membrane-bound receptor. Therefore, the K_D difference is likely to represent two sides of a coin. We speculate that both membrane-bound ligands and receptors might be essential for obtaining the binding affinities of the cell-cell contact based Eph/ephrin interactions.

This work represents the first attempt to elucidate the critical role of N-glycosylation in Eph/ephrin specific interactions. At the molecular level, cell-based FCM assays revealed that there is a two-order-of-magnitude binding affinities difference of EphB2 toward ephrin-A5 (K_D = 111.9 nM) and ephrin-B2 (K_D = 3.526 nM). The N-glycosylation deficient mutant diminished the EphB2 binding specificities to ephrin-A5 (K_D = 32.29 nM) and ephrin-B2 (K_D = 29.91 nM). At the cell level, the N-glycosylation deficient mutant of EphB2 abolished the EphB2 binding specificities to ephrin-A5 and ephrin-B2 in terms of cell retraction (Figure 6). At the tissue level, N-glycosylation of EphB2 robustly exists during neuron development (Figures 3A, 7A, and 7B). The N-glycosylation deficient mutant of EphB2 affected dendritic spine formation in cultured hippocampal neurons (Figures 7C–7E), which suggested that N-glycosylation is physiologically important for neuronal development. In addition, sequence alignment analysis showed that N-glycosylation modifications are highly conserved and commonly exist in Eph receptors (Figures S6). Gain-of-function mutations of EphB6 restored its ephrin-B2 binding ability. Furthermore, mutation of N-glycosylation deficient mutations are found in various cancer patients, indicating that N-glycosylation modification may also be involved in the process of different cancers (Figure 5E). Thus, N-glycosylation seems to be a critical and general regulator of Eph receptors' ligand recognition.

N-glycosylation in the extracellular domain contributes to the selective binding of EphB2 to ephrin-A5/B2. The glycosylation pattern of the purified EphB2 ectodomain was characterized by mass spectrometry. We listed the most prominent glycan and chemical structures attached to the four N-glycosylation sites within the EphB2 ectodomain (Figures S3A and S3B). The diameters of the proposed sugar chains exceed 10 Å (Figure S3C), potentially generating steric hindrance once the

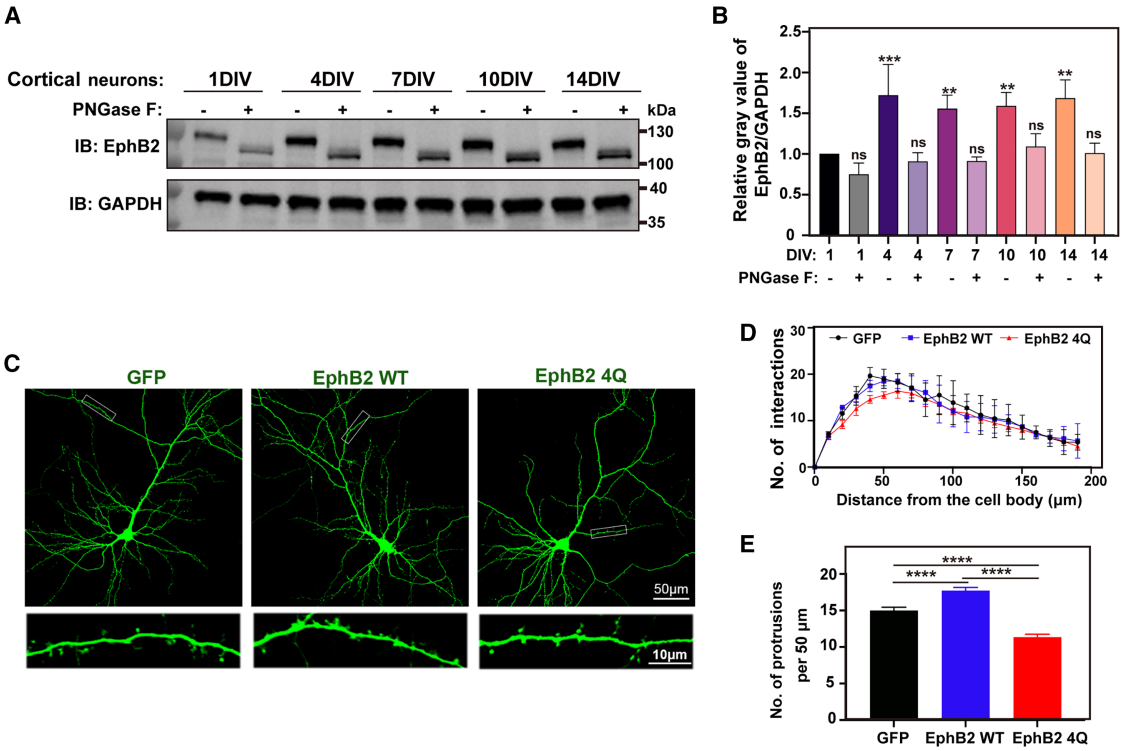

Figure 7. N-glycosylation of EphB2 is required for the development of dendritic spines

(A) Western blot results of endogenous EphB2 before/after PNGase F treatment in rat primary cortical neurons from DIV1 to DIV14.

(B) Relative EphB2 expression level of (A). The relative EphB2 expression level is represented by the ratio of EphB2/GAPDH, with DIV1 set to 1. Statistical analysis was performed by one-way ANOVA with Dunnett's post hoc test; ns, not significant; $^{*}p < 0.05$; $^{**}p < 0.01$, $^{***}p < 0.001$ compared with DIV1 ($n = 3$).

(C) Representative images of cultured hippocampal neurons at 14 DIV. The morphology of transfected neurons with GFP control, EphB2 WT, and EphB2 4Q was visualized by GFP. Scale bar: 50 μm for top and 10 μm for bottom.

(D) Sholl analysis demonstrates that no significant difference was found in dendritic morphology between cultured DIV14 EphB2 WT and EphB2 4Q neurons ($n = 3$; 20 neurons imaged per panel; one-way ANOVA; Tukey's post-hoc multiple comparisons test).

(E) The number of dendritic protrusions was quantified ($n = 3$, 20 neurons imaged per panel; one-way ANOVA; Tukey's post-hoc multiple comparisons test; $^{****}p < 0.0001$).

All data are represented as mean ± SD.

glycosylation sites are adjacent to interaction interfaces. Besides, glycans could also interact with cell membrane, thereby changing the orientation of receptor on the membrane and accessibility to the ligand-receptor interaction interface.[26,37,50]

Limitations of the study

The observation that N-glycosylation affects the Eph/ephrin binding selectivity opens an entry point to understand complex Eph/ephrin interaction preference. However, it would be more concretely grounded with supplied with the glycosylated ephrin-Eph protein complexes. Methodologically, although FCM is a useful tool to measure the accurate ligand-receptor binding affinities in membrane environments, it is not suitable for high throughput assays. The remainder Eph/ephrin interactions are needed to be testified by FCM analysis in the future.

RESOURCE AVAILABILITY

Lead contact

Further information and requests for resources and reagents should be directed to and will be fulfilled by the lead contact, Wei Liu (liuwei@sphmc.org).

Materials availability

Any materials generated in this study are available from the lead contact with a completed materials transfer agreement.

Data and code availability

- All data reported in this paper will be shared by the lead contact upon request.
- This paper does not report original code.
- Any additional information required to reanalyze the data reported in this paper is available from the lead contact upon request.

ACKNOWLEDGMENTS

This work was supported by the National Natural Science Foundation of China (no. 31870746), Shenzhen Fundamental Research Program (JCYJ20200109140414636 and JCYJ20230807145103007) and Guangdong Basic and Applied Basic Research Foundation (2021A1515010796, 2022A1515010666 and 2025A1515010736) to W.L., NSFC-RGC Joint Research Scheme (32061160472) to Y.C., National Natural Science Foundation of China (T2394511) to W.C., and National Natural Science Foundation of China (12002307) to W.H. We thank Professor Ting Xie from The Hong Kong University of Science and Technology for critical reading and helpful discussion of the manuscript.

AUTHOR CONTRIBUTIONS

Conceptualization, W.L. and C.L.; methodology, C.L., L.Y., Y.Y., D.Z., and W. H.; validation, C.L., L.Y., Y.Y., and D.Z.; investigation, C.L. and L.Y.; resources, W.H., Y.D., K.Z., and W.C.; formal analysis, C.L., W.L., K.X., and Y.C.; writing – original draft, C.L.; writing – review & editing, C.L., W.L., K.X., and Y.C.; supervision, Y.C., K.X., and W.L.; funding acquisition, W.H., Y.C., and W.L. All authors have read and agreed to the published version of the manuscript.

DECLARATION OF INTERESTS

The authors declare no competing interests.

STAR★METHODS

Detailed methods are provided in the online version of this paper and include the following:

- KEY RESOURCES TABLE
- EXPERIMENTAL MODEL AND STUDY PARTICIPANT DETAILS
  - Cell lines and primary cells
  - *In vivo* studies: Mice
- METHOD DETAILS
  - Reagents
  - Ethics statement
  - Plasmid construction and protein purification
  - Plasmids transfection
  - Lentivirus assembly and transduction
  - Ligand-induced ligand/receptor colocalization
  - HEK293T cell rounding assay
  - Glycosylation analysis of EphB2
  - Flow-cytometry-based Eph/ephrin binding assay
  - Flow cytometry analysis and calibration
  - Cell-based EphB2 kinase activation assay
  - Liposome-binding assay
- QUANTIFICATION AND STATISTICAL ANALYSIS

SUPPLEMENTAL INFORMATION

Supplemental information can be found online at https://doi.org/10.1016/j.isci.2025.112386.

Received: July 12, 2024
Revised: October 25, 2024
Accepted: April 4, 2025
Published: April 8, 2025

REFERENCES

1. Pasquale, E.B. (2005). Eph receptor signalling casts a wide net on cell behaviour. Nat. Rev. Mol. Cell Biol. *6*, 462–475. https://doi.org/10.1038/nrm1662.
2. Kullander, K., Mather, N.K., Diella, F., Dottori, M., Boyd, A.W., and Klein, R. (2001). Kinase-dependent and kinase-independent functions of EphA4 receptors in major axon tract formation *in vivo*. Neuron *29*, 73–84. https://doi.org/10.1016/s0896-6273(01)00181-7.
3. Marston, D.J., Dickinson, S., and Nobes, C.D. (2003). Rac-dependent trans-endocytosis of ephrinBs regulates Eph-ephrin contact repulsion. Nat. Cell Biol. *5*, 879–888. https://doi.org/10.1038/ncb1044.
4. Zimmer, M., Palmer, A., Köhler, J., and Klein, R. (2003). EphB-ephrinB bi-directional endocytosis terminates adhesion allowing contact mediated repulsion. Nat. Cell Biol. *5*, 869–878. https://doi.org/10.1038/ncb1045.
5. Shi, X., Lingerak, R., Herting, C.J., Ge, Y., Kim, S., Toth, P., Wang, W., Brown, B.P., Meiler, J., Sossey-Alaoui, K., et al. (2023). Time-resolved live-cell spectroscopy reveals EphA2 multimeric assembly. Science (New York, N.Y.) *382*, 1042–1050. https://doi.org/10.1126/science.adg5314.
6. Flanagan, J.G., Gale, N.W., Hunter, T., Pasquale, E.B., and Tessier-Lavigne, M. (1997). Unified nomenclature for Eph family receptors and their ligands, the ephrins. Eph Nomenclature Committee. Cell *90*, 403–404. https://doi.org/10.1016/s0092-8674(00)80500-0.
7. Rohani, N., Parmeggiani, A., Winklbauer, R., and Fagotto, F. (2014). Variable combinations of specific ephrin ligand/Eph receptor pairs control embryonic tissue separation. PLoS Biol. *12*, e1001955. https://doi.org/10.1371/journal.pbio.1001955.
8. Bai, J., Wang, Y.J., Liu, L., and Zhao, Y.L. (2014). Ephrin B2 and EphB4 selectively mark arterial and venous vessels in cerebral arteriovenous malformation. J. Int. Med. Res. *42*, 405–415. https://doi.org/10.1177/0300060513478091.
9. Adams, R.H., Wilkinson, G.A., Weiss, C., Diella, F., Gale, N.W., Deutsch, U., Risau, W., and Klein, R. (1999). Roles of ephrinB ligands and EphB receptors in cardiovascular development: demarcation of arterial/venous domains, vascular morphogenesis, and sprouting angiogenesis. Genes Dev. *13*, 295–306. https://doi.org/10.1101/gad.13.3.295.
10. Kayser, M.S., Nolt, M.J., and Dalva, M.B. (2008). EphB receptors couple dendritic filopodia motility to synapse formation. Neuron *59*, 56–69. https://doi.org/10.1016/j.neuron.2008.05.007.
11. Pasquale, E.B. (2024). Eph receptors and ephrins in cancer progression. Nat. Rev. Cancer *24*, 5–27. https://doi.org/10.1038/s41568-023-00634-x.
12. Al Rahim, M., Yoon, Y., Dimovasili, C., Shao, Z., Huang, Q., Zhang, E., Kezunovic, N., Chen, L., Schaffner, A., Huntley, G.W., et al. (2020). Presenilin1 familial Alzheimer disease mutants inactivate EFNB1- and BDNF-dependent neuroprotection against excitotoxicity by affecting neuroprotective complexes of N-methyl-d-aspartate receptor. Brain Commun. *2*, fcaa100. https://doi.org/10.1093/braincomms/fcaa100.
13. Cai, C., Zhang, M., Liu, L., Zhang, H., Guo, Y., Lan, T., Xu, Y., Ma, P., and Li, S. (2022). ADAM10-cleaved ephrin-A5 contributes to prostate cancer metastasis. Cell Death Dis. *13*, 453. https://doi.org/10.1038/s41419-022-04893-8.
14. Li, M., Nishio, S.Y., Naruse, C., Riddell, M., Sapski, S., Katsuno, T., Hikita, T., Mizapourshafiyi, F., Smith, F.M., Cooper, L.T., et al. (2020). Digenic inheritance of mutations in EPHA2 and SLC26A4 in Pendred syndrome. Nat. Commun. *11*, 1343. https://doi.org/10.1038/s41467-020-15198-9.
15. Noberini, R., Rubio de la Torre, E., and Pasquale, E.B. (2012). Profiling Eph receptor expression in cells and tissues: a targeted mass spectrometry approach. Cell Adhes. Migrat. *6*, 102–112. https://doi.org/10.4161/cam.19620.
16. Himanen, J.P., Chumley, M.J., Lackmann, M., Li, C., Barton, W.A., Jeffrey, P.D., Vearing, C., Geleick, D., Feldheim, D.A., Boyd, A.W., et al. (2004). Repelling class discrimination: ephrin-A5 binds to and activates EphB2 receptor signaling. Nat. Neurosci. *7*, 501–509. https://doi.org/10.1038/nn1237.
17. Henkemeyer, M., Itkis, O.S., Ngo, M., Hickmott, P.W., and Ethell, I.M. (2003). Multiple EphB receptor tyrosine kinases shape dendritic spines in the hippocampus. J. Cell Biol. *163*, 1313–1326. https://doi.org/10.1083/jcb.200306033.
18. Mao, Y.T., Zhu, J.X., Hanamura, K., Iurilli, G., Datta, S.R., and Dalva, M.B. (2018). Filopodia Conduct Target Selection in Cortical Neurons Using Differences in Signal Kinetics of a Single Kinase. Neuron *98*, 767–782.e8. https://doi.org/10.1016/j.neuron.2018.04.011.
19. Ojosnegros, S., Cutrale, F., Rodríguez, D., Otterstrom, J.J., Chiu, C.L., Hortigüela, V., Tarantino, C., Seriola, A., Mieruszynski, S., Martínez, E., et al. (2017). Eph-ephrin signaling modulated by polymerization and condensation of receptors. Proc. Natl. Acad. Sci. USA *114*, 13188–13193. https://doi.org/10.1073/pnas.1713564114.
20. Jiang, Y., Thienpont, B., Sapuru, V., Hite, R.K., Dittman, J.S., Sturgis, J.N., and Scheuring, S. (2022). Membrane-mediated protein interactions drive

membrane protein organization. Nat. Commun. *13*, 7373. https://doi.org/10.1038/s41467-022-35202-8.

21. Gurdap, C.O., Wedemann, L., Sych, T., and Sezgin, E. (2022). Influence of the extracellular domain size on the dynamic behavior of membrane proteins. Biophys. J. *121*, 3826–3836. https://doi.org/10.1016/j.bpj.2022.09.010.
22. Chavent, M., Seiradake, E., Jones, E.Y., and Sansom, M.S.P. (2016). Structures of the EphA2 Receptor at the Membrane: Role of Lipid Interactions. Structure *24*, 337–347. https://doi.org/10.1016/j.str.2015.11.008.
23. Kaszuba, K., Grzybek, M., Orłowski, A., Danne, R., Róg, T., Simons, K., Coskun, Ü., and Vattulainen, I. (2015). N-Glycosylation as determinant of epidermal growth factor receptor conformation in membranes. Proc. Natl. Acad. Sci. USA *112*, 4334–4339. https://doi.org/10.1073/pnas.1503262112.
24. Chandler, K.B., Leon, D.R., Kuang, J., Meyer, R.D., Rahimi, N., and Costello, C.E. (2019). N-Glycosylation regulates ligand-dependent activation and signaling of vascular endothelial growth factor receptor 2 (VEGFR2). J. Biol. Chem. *294*, 13117–13130. https://doi.org/10.1074/jbc.RA119.008643.
25. Contessa, J.N., Bhojani, M.S., Freeze, H.H., Rehemtulla, A., and Lawrence, T.S. (2008). Inhibition of N-linked glycosylation disrupts receptor tyrosine kinase signaling in tumor cells. Cancer. Res. *68*, 3803–3809. https://doi.org/10.1158/0008-5472.Can-07-6389.
26. Azimzadeh Irani, M., Kannan, S., and Verma, C. (2017). Role of N-glycosylation in EGFR ectodomain ligand binding. Proteins *85*, 1529–1549. https://doi.org/10.1002/prot.25314.
27. Taylor, E.S., Pol-Fachin, L., Lins, R.D., and Lower, S.K. (2017). Conformational stability of the epidermal growth factor (EGF) receptor as influenced by glycosylation, dimerization and EGF hormone binding. Proteins *85*, 561–570. https://doi.org/10.1002/prot.25220.
28. Liu, K., Tan, S., Jin, W., Guan, J., Wang, Q., Sun, H., Qi, J., Yan, J., Chai, Y., Wang, Z., et al. (2020). N-glycosylation of PD-1 promotes binding of camrelizumab. EMBO Rep. *21*, e51444. https://doi.org/10.15252/embr.202051444.
29. Huang, Y.L., Liang, C.Y., Labitzky, V., Ritz, D., Oliveira, T., Cumin, C., Estermann, M., Lange, T., Everest-Dass, A.V., and Jacob, F. (2021). Site-specific N-glycosylation of integrin α2 mediates collagen-dependent cell survival. iScience *24*, 103168. https://doi.org/10.1016/j.isci.2021.103168.
30. Xu, Y., Robev, D., Saha, N., Wang, B., Dalva, M.B., Xu, K., Himanen, J.P., and Nikolov, D.B. (2021). The Ephb2 Receptor Uses Homotypic, Head-to-Tail Interactions within Its Ectodomain as an Autoinhibitory Control Mechanism. Int. J. Mol. Sci. *22*, 10473. https://doi.org/10.3390/ijms221910473.
31. Forbes, S.A., Beare, D., Boutselakis, H., Bamford, S., Bindal, N., Tate, J., Cole, C.G., Ward, S., Dawson, E., Ponting, L., et al. (2017). COSMIC: somatic cancer genetics at high-resolution. Nucleic Acids Res. *45*, D777-d783. https://doi.org/10.1093/nar/gkw1121.
32. Schaupp, A., Sabet, O., Dudanova, I., Ponserre, M., Bastiaens, P., and Klein, R. (2014). The composition of EphB2 clusters determines the strength in the cellular repulsion response. J. Cell Biol. *204*, 409–422. https://doi.org/10.1083/jcb.201305037.
33. Lawrenson, I.D., Wimmer-Kleikamp, S.H., Lock, P., Schoenwaelder, S.M., Down, M., Boyd, A.W., Alewood, P.F., and Lackmann, M. (2002). Ephrin-A5 induces rounding, blebbing and de-adhesion of EphA3-expressing 293T and melanoma cells by CrkII and Rho-mediated signalling. J. Cell Sci. *115*, 1059–1072. https://doi.org/10.1242/jcs.115.5.1059.
34. Ethell, I.M., Irie, F., Kalo, M.S., Couchman, J.R., Pasquale, E.B., and Yamaguchi, Y. (2001). EphB/syndecan-2 signaling in dendritic spine morphogenesis. Neuron *31*, 1001–1013. https://doi.org/10.1016/s0896-6273(01)00440-8.
35. Wang, Y., Shang, Y., Li, J., Chen, W., Li, G., Wan, J., Liu, W., and Zhang, M. (2018). Specific Eph receptor-cytoplasmic effector signaling mediated by SAM-SAM domain interactions. Elife *7*, e35677. https://doi.org/10.7554/eLife.35677.
36. Klaver, E., Zhao, P., May, M., Flanagan-Steet, H., Freeze, H.H., Gilmore, R., Wells, L., Contessa, J., and Steet, R. (2019). Selective inhibition of N-linked glycosylation impairs receptor tyrosine kinase processing. Dis. Model. Mech. *12*, dmm039602. https://doi.org/10.1242/dmm.039602.
37. Matoba, K., Mihara, E., Tamura-Kawakami, K., Miyazaki, N., Maeda, S., Hirai, H., Thompson, S., Iwasaki, K., and Takagi, J. (2017). Conformational Freedom of the LRP6 Ectodomain Is Regulated by N-glycosylation and the Binding of the Wnt Antagonist Dkk1. Cell Rep. *18*, 32–40. https://doi.org/10.1016/j.celrep.2016.12.017.
38. Hunter, S.A., and Cochran, J.R. (2016). Cell-Binding Assays for Determining the Affinity of Protein-Protein Interactions: Technologies and Considerations. Methods Enzymol. *580*, 21–44. https://doi.org/10.1016/bs.mie.2016.05.002.
39. Kozma, E., Kumar, T.S., Federico, S., Phan, K., Balasubramanian, R., Gao, Z.G., Paoletta, S., Moro, S., Spalluto, G., and Jacobson, K.A. (2012). Novel fluorescent antagonist as a molecular probe in A(3) adenosine receptor binding assays using flow cytometry. Biochem. Pharmacol. *83*, 1552–1561. https://doi.org/10.1016/j.bcp.2012.02.019.
40. Maguire, J.J., Kuc, R.E., and Davenport, A.P. (2012). Radioligand binding assays and their analysis. Methods Mol. Biol. *897*, 31–77. https://doi.org/10.1007/978-1-61779-909-9_3.
41. Paton, W.D., and Rang, H.P. (1965). THE UPTAKE OF ATROPINE AND RELATED DRUGS BY INTESTINAL SMOOTH MUSCLE OF THE GUINEA-PIG IN RELATION TO ACETYLCHOLINE RECEPTORS. Proc. R. Soc. Lond. B Biol. Sci. *163*, 1–44. https://doi.org/10.1098/rspb.1965.0058.
42. Miao, H., Burnett, E., Kinch, M., Simon, E., and Wang, B. (2000). Activation of EphA2 kinase suppresses integrin function and causes focal-adhesion-kinase dephosphorylation. Nat. Cell Biol. *2*, 62–69. https://doi.org/10.1038/35000008.
43. Tognolini, M., Incerti, M., Hassan-Mohamed, I., Giorgio, C., Russo, S., Bruni, R., Lelli, B., Bracci, L., Noberini, R., Pasquale, E.B., et al. (2012). Structure-activity relationships and mechanism of action of Eph-ephrin antagonists: interaction of cholanic acid with the EphA2 receptor. ChemMedChem *7*, 1071–1083. https://doi.org/10.1002/cmdc.201200102.
44. Zarnitsyna, V., and Zhu, C. (2012). T cell triggering: insights from 2D kinetics analysis of molecular interactions. Phys. Biol. *9*, 045005. https://doi.org/10.1088/1478-3975/9/4/045005.
45. Chen, W., Zarnitsyna, V.I., Sarangapani, K.K., Huang, J., and Zhu, C. (2008). Measuring Receptor-Ligand Binding Kinetics on Cell Surfaces: From Adhesion Frequency to Thermal Fluctuation Methods. Cell. Mol. Bioeng. *1*, 276–288. https://doi.org/10.1007/s12195-008-0024-8.
46. Xu, C., and Ng, D.T.W. (2015). Glycosylation-directed quality control of protein folding. Nat. Rev. Mol. Cell Biol. *16*, 742–752. https://doi.org/10.1038/nrm4073.
47. Poitz, D.M., Ende, G., Stütz, B., Augstein, A., Friedrichs, J., Brunssen, C., Werner, C., Strasser, R.H., and Jellinghaus, S. (2015). EphrinB2/EphA4-mediated activation of endothelial cells increases monocyte adhesion. Mol. Immunol. *68*, 648–656. https://doi.org/10.1016/j.molimm.2015.10.009.
48. Gale, N.W., Holland, S.J., Valenzuela, D.M., Flenniken, A., Pan, L., Ryan, T.E., Henkemeyer, M., Strebhardt, K., Hirai, H., Wilkinson, D.G., et al. (1996). Eph receptors and ligands comprise two major specificity subclasses and are reciprocally compartmentalized during embryogenesis. Neuron *17*, 9–19. https://doi.org/10.1016/s0896-6273(00)80276-7.
49. Bowden, T.A., Aricescu, A.R., Nettleship, J.E., Siebold, C., Rahman-Huq, N., Owens, R.J., Stuart, D.I., and Jones, E.Y. (2009). Structural plasticity of eph receptor A4 facilitates cross-class ephrin signaling. Structure *17*, 1386–1397. https://doi.org/10.1016/j.str.2009.07.018.
50. Torreno-Pina, J.A., Castro, B.M., Manzo, C., Buschow, S.I., Cambi, A., and Garcia-Parajo, M.F. (2014). Enhanced receptor-clathrin interactions induced by N-glycan-mediated membrane micropatterning. Proc. Natl.

Acad. Sci. USA *111*, 11037–11042. https://doi.org/10.1073/pnas.1402041111.

51. Subedi, G.P., Johnson, R.W., Moniz, H.A., Moremen, K.W., and Barb, A. W. (2015). High Yield Expression of Recombinant Human Proteins with the Transient Transfection of HEK293 Cells in Suspension. J. Vis. Exp. *106*, e53568. https://doi.org/10.3791/53568.

52. Fu, W.Y., Chen, Y., Sahin, M., Zhao, X.S., Shi, L., Bikoff, J.B., Lai, K.O., Yung, W.H., Fu, A.K.Y., Greenberg, M.E., and Ip, N.Y. (2007). Cdk5 regulates EphA4-mediated dendritic spine retraction through an ephexin1-dependent mechanism. Nat. Neurosci. *10*, 67–76. https://doi.org/10.1038/nn1811.

53. Colby, D.W., Kellogg, B.A., Graff, C.P., Yeung, Y.A., Swers, J.S., and Wittrup, K.D. (2004). Engineering antibody affinity by yeast surface display. Methods Enzymol. *388*, 348–358. https://doi.org/10.1016/s0076-6879(04)88027-3.

54. Mittag, A., and Tárnok, A. (2009). Basics of standardization and calibration in cytometry–a review. J. Biophot. *2*, 470–481. https://doi.org/10.1002/jbio.200910033.

55. Wen, W., Liu, W., Yan, J., and Zhang, M. (2008). Structure basis and unconventional lipid membrane binding properties of the PH-C1 tandem of rho kinases. J. Biol. Chem. *283*, 26263–26273. https://doi.org/10.1074/jbc.M803417200.

56. Yan, J., Wen, W., Xu, W., Long, J.F., Adams, M.E., Froehner, S.C., and Zhang, M. (2005). Structure of the split PH domain and distinct lipid-binding properties of the PH-PDZ supramodule of alpha-syntrophin. EMBO J. *24*, 3985–3995. https://doi.org/10.1038/sj.emboj.7600858.

57. Langhammer, C.G., Previtera, M.L., Sweet, E.S., Sran, S.S., Chen, M., and Firestein, B.L. (2010). Automated Sholl analysis of digitized neuronal morphology at multiple scales: Whole cell Sholl analysis versus Sholl analysis of arbor subregions. Cytometry *77*, 1160–1168. https://doi.org/10.1002/cyto.a.20954.

STAR★METHODS

KEY RESOURCES TABLE

REAGENT or RESOURCE	SOURCE	IDENTIFIER
Antibodies		
DYKDDDDK Tag (D6W5B) Rabbit mAb	Cell Signaling Technology	Cat#14793
HA-Tag (C29F4) Rabbit mAb	Cell Signaling Technology	Cat# 3724
GAPDH (14C10) Rabbit mAb	Cell Signaling Technology	Cat#2118
Anti-rabbit IgG, HRP-linked Antibody	Cell Signaling Technology	Cat#7074
Anti-mouse IgG, HRP-linked Antibody	Cell Signaling Technology	Cat#7076
Human/Mouse EphB2 Antibody	R&D SYSTEMS	Cat#AF467
Goat IgG (H+L) PE-conjugated Antibody	R&D SYSTEMS	Cat# F0107
Anti-Phosphotyrosine Antibody	Merck Millipore	Cat#05-1050-M
Alexa Fluor™ 647 Streptavidin Conjugate	Thermo Fisher Scientific	Cat#S21374
Goat anti-Mouse IgG (H+L) Cross-Adsorbed Secondary Antibody, Alexa Fluor™ 488	Thermo Fisher Scientific	Cat#A-11001; RRID: AB_2534069
Goat anti-Rabbit IgG (H+L) Cross-Adsorbed Secondary Antibody, Alexa Fluor™ 555	Thermo Fisher Scientific	Cat#A-21428; RRID: AB_2535849
Goat anti-Rabbit IgG (H+L) Cross-Adsorbed Secondary Antibody, Alexa Fluor™ 555	Thermo Fisher Scientific	Cat#A-21428; RRID: AB_2535849
Phospho-EphB1/EphB2 (Tyr594, Tyr604) Polyclonal Antibody	Thermo Fisher Scientific	Cat#PA5-40236; RRID: AB_2609042
HRP-conjugated Affinipure Donkey Anti-Goat IgG(H+L)	Proteintech	Cat#SA00001-3; RRID: AB_2890882
Chemicals, peptides, and recombinant proteins		
Polybrene	Solarbio	H8761
Lipo8000™ Transfection Reagent	Beyotime	C0533
Polyethylenimine Linear	Polysciences	24765-1
PNGase F	New England BioLabs	P0704
ANTI-FLAG® M2 Affinity Gel	Sigma-Aldrich	A2220-1
Brain Extract from bovine brain	Sigma-Aldrich	B1502
Critical commercial assays		
Universal Virus Concentration Kit	Beyotime	C2901
Quantumtm MESF microsphere kits	Bangs Laboratories	PSD818
Deposited data		
No		
Experimental models: Cell lines		
Expi293F	Gibco	CVCL_D615
Rat primary hippocampal neurons	This lab	
Rat primary cortical neurons	This lab	
HEK293T	ATCC	CVCL_0063
Experimental models: Organisms/strains		
Mice (C57/B6J)	Cyagen Biosciences	
Rat (SD)	Cyagen Biosciences	
Oligonucleotides		
See Table S1		
Recombinant DNA		
Plasmid: pcDNA™ 3.4 TOPO™	Thermo Fisher Scientific	A14697
pHAGE vector	kindly provided by Dr. Qiming Sun, Zhejiang University	

(*Continued on next page*)

Continued

REAGENT or RESOURCE	SOURCE	IDENTIFIER
Plasmid: psPAX2	Addgene	Cat#12260
Plasmid: pMD2.G	Addgene	Cat#12259
Software and algorithms		
GraPad Prism 10.0	Grapad software	https://www.graphpad.com/demos/
Image J	National Institutes of Health	https://imagej.en.softonic.com/
FlowJo v10	BD Biosciences	https://www.bdbiosciences.com/zh-cn/products/software/flowjo-v10-software
Other		
COSMIC cancer somatic mutation database	COSMIC	http://cancer.sanger.ac.uk/cosmic
Predict N-linked glycosylation sites in human proteins	NetNGlyc - 1.0	https://services.healthtech.dtu.dk/services/NetNGlyc-1.0/
Sequence alignment	CLUSTALW	https://www.genome.jp/tools-bin/clustalw
Sequence alignment	ESPript3.0	https://espript.ibcp.fr/ESPript/ESPript/

EXPERIMENTAL MODEL AND STUDY PARTICIPANT DETAILS

Cell lines and primary cells

HEK293T (RRID: CVCL_0063; female) cells were purchased from American Type Culture Collection (ATCC). HEK293T cells were cultured in DMEM medium supplemented with 10% Fetal Bovine Serum (FBS, Gibco) and 1% penicillin/streptomycin (PS, 100 U/ml, Gibco). Plasmids were transfected into HEK 293T cells using Lipo8000^{TM} Transfection Reagent following the manufacturer's instructions (Beyotime). Expi293F cells (RRID: CLCL_D615; female) were purchased from Gibco and grown in suspension on a platform shaker rotating at 120 rpm using Balanced CD 293 Medium (Life Technologies, CW001). The cells were maintained at 37°C in a humidified atmosphere with 8% CO_2. Primary hippocampal and cortical neurons were dissociated from 18.5-day rat embryos (the sex/gender of the embryos was not distinguished, as the influence of sex/gender was not applicable in this study) and fed with Neurobasal Plus Medium with 2% B-27 Plus Supplement. The HEK293T cell lines were authenticated through short tandem repeat (STR) analysis and confirmed to be mycoplasma-free through PCR testing.

In vivo studies: Mice

Wild-type 10-day-old (C57/B6J; male mice; approximately 6g) and adult (C57/B6J; 6-8 week; male mice; approximately 6g) mice were purchased from Cyagen Biosciences. During transportation, the mice were provided with jelly and standard chow to maintain hydration and nutrition. Upon arrival, the mice were euthanized for hippocampus tissues collection. The sex/gender of the mice was not distinguished, as the influence of sex/gender was not applicable in this study.

METHOD DETAILS

Reagents

The reagents used in the study are listed in the key resources table.

Ethics statement

All animal procedures were approved by the Institutional Animal Care and Use Committee of Guangdong Provincial Key Laboratory of Brain Science, Disease and Drug Development, in accordance with the National Care and Use of Laboratory Animals Guidelines (China). All animal experiments were conducted ethically according to the Guide for the Care and Use of Laboratory Animal guidelines (Ethics approval number HKUST-AUP-2023-0001).

Plasmid construction and protein purification

The extracellular domain of murine EphB2 (residues 19-543; GenBank accession number NP_034272.1) and the receptor binding domains of murine ephrin-B2 (residues 30-170; GenBank accession number NP_034241.2) and ephrin-A5 (residues 28-164; GenBank accession number NP_997537.1) were cloned into a modified pCDNA3.4 TOPO mammalian expression vector (Thermo Fisher Scientific, A14697), with HA secretion signal and C-terminal His_8 as an affinity tag. Additionally, ephrin-B2 and ephrin-A5 are appended with an extra C-terminal Avi tag. Mutations were introduced using a standard PCR-based mutagenesis method and underwent thorough sequence verification.

Recombinant protein expression was achieved by transiently transfecting human Expi293F cell lines with the mammalian expression vector. The medium containing the secreted fusion protein was collected 72 to 96 hours post-transfection and subsequently

loaded onto a Ni Sepharose™ excel affinity column (Cytiva™). The ensuing step involved meticulous purification through gel filtration chromatography, using a Superdex-200 column (AKTA™, Cytiva™). Furthermore, for ephrin-B2 and ephrin-A5, S200-purified ephrin-A5 and ephrin-B2 proteins were biotinylated using the Avi tag and the BirA enzyme in PBS buffer (comprising 5 mM $MgCl_2$, 2 mM ATP, 0.2 mM D-Biotin, 1 μM homemade BirA). The biotinylation was conducted at 30°C for 1 hour. An additional purification step was conducted using anion-exchange chromatography (HiTrap CaptoQ, Cytiva™). The purified proteins were obtained in a buffer comprising 50 mM Tris-HCl (pH 8.0), 150 mM NaCl, 1 mM DTT, and 1 mM EDTA, establishing an optimal biochemical environment for subsequent studies and analyses.

Plasmids transfection

Twenty-four hours before transfection, Expi293F cells were split to a density of $\sim 1.5 \times 10^6$ cells/ml and cultured overnight in the CO_2 incubator with shaking at 37°C. The cell density should reach $\sim 3 \times 10^6$ after 24 hours and then be subjected to transfection. For transfection, the expression vector plasmid DNA was added to the cells at a final concentration of 2 μg/ml, and PEI (Polysciences, 24765-1) was added to a final concentration of 3 μg/ml of transfection volume.[51] Subsequently, harvesting was performed 72-96 hours post-transfection. Primary hippocampal and cortical neurons were seeded at the density of 1×10^5 per coverslip for calcium transfection. These neurons at DIV11 were transfected with the empty vector, EphB2, and EphB2 4Q together with GFP at the ratio of 3:1 using calcium phosphate precipitation.[52] Three days post-transfection, the neurons at DIV14 were fixed with 4% paraformaldehyde and the images of dendritic and spine morphology were obtained by confocal microscopy (Zeiss LSM 900).

Lentivirus assembly and transduction

Lentivirus carrying the following constructs were generated through infecting HEK293T cells using Lipo8000 (Beyotime, C0533): pHAGE-EphB2-IRES-Green, pHAGE-EphB2 N265Q-IRES-Green, pHAGE-EphB2 N336Q-IRES-Green, pHAGE-EphB2 N428Q-IRES-Green, pHAGE-EphB2 N482Q-IRES-Green, pHAGE-EphB2 N265, N336Q-IRES-Green, pHAGE-EphB2 N428, N482Q-IRES-Green, pHAGE-EphB2 4Q-IRES-Green, pHAGE-EphB3-IRES-Green, pHAGE-EphB4-IRES-Green, pHAGE-EphB6-IRES-Green, pHAGE-EphB6 NSS^{527}-IRES-Green, pHAGE-EphB6 $^{305}NDS^{307}/^{527}NSS^{529}$-IRES-Green, pHAGE vector was kindly provided by Dr. Qiming Sun, Zhejiang University. Simultaneously, packaging expression vectors psPAX2 and pMD2.G were co-transfected. After transfection, the supernatant medium was refreshed 24 hours later and subsequently collected at 24-hour intervals. The collected medium containing lentivirus was filtered through 0.45μm filters and concentrated by Universal Virus Concentration Kit (Beyotime, C2901). Subsequently, Expi293F cells were transduced with recombinant lentivirus particles in the presence of 10 μg/ml polybrene (Solarbio, H8761). After a 72-hour incubation, positive cells were gated based on cell fluorescence using flow cytometry.

Ligand-induced ligand/receptor colocalization

Expi293F cells were transiently infected with lentivirus carrying EphB2 WT or different EphB2 N-glycosylation mutants (N265Q; N336Q; N428Q; N482Q; N265, N336Q; N428, N482Q; 4Q/N265, N336, N428, N482Q). The different N-glycosylation mutations did not affect the EphB2 protein expression level, confirmed by Western blot using an anti-EphB2 antibody (R&D SYSTEMS, AF467). After a 72-hour infection, biotinylated ephrin-A5 or ephrin-B2 proteins were pre-clustered with Streptavidin-Alexa 647 (Invitrogen, Inc.) for 1 hour at 4°C on a shaker in the dark. Subsequently, when comparing the binding abilities of EphB2 WT or N-glycosylation deficient EphB2 receptor cells to different ligands, the same flask of virus-infected cells was used. The infected cells were equally divided into several fractions, centrifuged, and incubated with different concentrations of pre-clustered ligands (0, 28.7, and 287 nM) for 15 minutes. After the binding reaction, the cells were washed twice with PBS, and following the final wash, the cells were resuspended and added to confocal dishes for imaging analysis. When comparing the binding abilities of different N-glycosylation mutants with ephrin ligands, equal numbers of cells (approximately 5×10^5) were incubated with the same concentrations of pre-clustered ligands for 15 minutes. After the binding reaction, the PBS washing steps were repeated, and the cells were resuspended and added to confocal dishes for live imaging conducted using a Zeiss LSM 710 confocal microscopy (63 × objective, N.A. 1.4). We scanned 7 × 7 grids with a total area of 863 × 863 μm using confocal microscopy. Image processing was performed using ZEN 2012, Fiji (the National Institutes of Health, NIH), and Adobe Photoshop (Adobe Systems, CA).

$$\text{The percentage of cells with EphB2 / ephrin colocalized } (\%) = \frac{\text{The number of Green cells with Red fluorescence)}}{\text{The number of Green Cells}}$$

HEK293T cell rounding assay

HEK293T cells were seeded into a glass-bottom cell culture dish (NEST, 801002) and transiently infected with lentivirus expressing GFP control, full-length EphB2 WT, or EphB2 4Q. One hour before starting of the cell rounding assays, cells were washed with D-PBS and incubated in medium (DMEM without phenol red, supplemented with 25mM HEPES, Invitrogen). Cells were then stimulated by pre-clustered ephrin-A5/B2, and changes in cell behavior were photographed.

Glycosylation analysis of EphB2

To confirm the glycosylation of the EphB2 protein, purified EphB2 extracellular protein and lysed protein from mouse brains or neurons were treated with PNGase F (New England BioLabs, P0704) according to the manufacturer's instructions. Subsequently,

Coomassie brilliant blue staining and Western blot experiments were performed to confirm the protein band shifts after de-glycosylation and the transformation of protein bands from smear to uniform. Additionally, conserved NXT/S (X is not Proline) motifs were identified among EphB2 receptors in different species through sequence alignment.

Flow-cytometry-based Eph/ephrin binding assay

To measure Eph/ephrin apparent binding affinities by flow cytometry, the presentation of EphB2 or its mutations on the mammalian cell surface was achieved through transient infection with the lentivirus mentioned above. Determining binding affinity (Kd) depends on establishing saturation curves, with the time to reach equilibrium and ligand depletion being crucial factors.[38] Prepare pre-clustered ligand proteins in advance, according to the method mentioned above. For the time to equilibrium, 0.5×10^6 Expi293F cells expressing EphB2 were incubated with 50 nM pre-clustered ephrin-A5 or ephrin-B2 proteins in a 500ul volume for varying time intervals to measure corresponding MFI values. A time equilibrium curve was fitted to determine the reaction time. For further saturation binding assays, 0.5×10^6 Expi293F cells expressing EphB2 were incubated with concentrations of biotinylated ephrin proteins ranging from 0.25 nM to 1000 nM at 4°C for 15 min in a 500 μl volume. After each time interval, cells were washed three times with ice-cold PBS. MFI values measured at different concentrations were used to fit a saturation binding curve for determining Kd. In nonspecific binding experiments, 0.5×10^6 Expi293F cells expressing the empty vector were used to measure MFI values at different concentrations, following the EphB2 protocol. Saturated binding curves were based on the condition that the total concentration of receptor is 10% of the ligand concentration.[38,53]

Flow cytometry analysis and calibration

Quantum^{tm} MESF (Molecules of Equivalent Soluble Fluorochrome) microsphere kits (Bangs Laboratories, Fishers, IN) were utilized to standardize fluorescence intensity units for quantitative fluorescence cytometry applications. The Quantum^{TM} MESF Alexa Fluor-647 MESF beads included one blank microsphere population and four microsphere populations surface-labeled with 647 in increasing amounts. The fluorescent bead standards were analyzed on the same day, using the same instrument, and at identical fluorescence settings (PMT and voltage) as the stained cell samples. This established a calibration curve relating instrument channel values to standardized fluorescence intensity (MESF) units.[54] Cell samples were initially gated based on side scatter (SSC) and forward scatter (FSC) to exclude dead cells and debris. From the live gate, FSC height by SSC area was plotted to ensure single-cell analysis. The plot was then set for APC by FITC+ and gated on sample cells to acquire MFI values. To minimize the background signals, MFI values were adjusted by subtracting the value of APC by FITC-. The final MFI values were further converted into MESF values using the QuickCal program v3.0 (Bangs Laboratories, Inc., Fishers, IN). Data were collected using a Beckman Coulter CytoFLEX S (Beckman, Brea, CA) with excitation wavelengths at 488, 561 and 638 nm through software, obtaining 5000 gated events for a sample to derive MFI value. The instrument underwent daily quality testing using beads. Data analysis was performed using FlowJo software (v10.8.1).

Cell-based EphB2 kinase activation assay

Expi293F cells were transiently transfected with modified pcDNA3.4 plasmids containing a C-terminal 3 × FLAG tag, encoding either EphB2 WT or EphB2 mutants with mutations at glycosylation sites within the extracellular domain (N265, N336Q; N428, N482Q; N265, N336, N428, N482Q), following protocols as described above. After 72 hours of transfection, soluble ephrin-A5 and ephrin-B2 proteins were pre-clustered and added to 0.5 ml cell cultures containing 1×10^6 EphB2-expressing cells at concentrations ranging from 30 to 250 nM. The phosphorylation reaction was conducted at room temperature for 1 hour with gentle rotation. Then, proteins were extracted using lysis buffer (50 mM Tris-HCl, pH 7.4, 150 mM NaCl, 1 mM EDTA, 1% TritonX-100), supplemented with a protease inhibitor cocktail and phosphatase inhibitor. Cellular debris was removed by centrifugation at 12000 × g for 10 minutes at 4°C. The supernatant (40 μL) were saved as input, while the remaining supernatant was incubated with 40 μL agarose-bound purified mouse FLAG (Sigma; Cat#A2220) for 2 hours at 4°C with gentle rotation. After incubation, the beads were spun down at 5000 × g for 30 s at 4°C and washed thoroughly with 0.5 mL TBS buffer (50 mM Tris-HCl, pH 7.4, 150 mM NaCl) three times. Immunoprecipitated proteins were eluted with a 20 μL 2 × SDS loading buffer. Finally, proteins were subjected to SDS–polyacrylamide gel electrophoresis and then transferred to a PVDF membrane. Western blot analysis was performed with anti-phosphotyrosine (Merck Millipore, 05-1050-M) or anti-phospho-EphB1/EphB2 (Tyr594, Tyr604) antibodies. Signal detection was performed by iBright FL1000 (Invitrogen). For the detection of protein phosphorylation and expression levels in cultured cortical neurons, Carestream X-Ray Films were used and developed by an OPTIMAX X-ray film processor.

Liposome-binding assay

A liposome precipitation assay was performed in a manner similar to that described in a previous report.[55,56] The stock solution of liposomes was prepared by resuspending total bovine brain lipids extracted using Folch fraction I (Sigma B1502) at a concentration of 5 mg/ml in a buffer containing 50 mM Tris (pH 7.5) and 150 mM NaCl. The sedimentation-based assay was conducted following the method described earlier. Briefly, liposome concentrations ranging from 0 to 3 mg/ml were incubated with 6.54 μM EphB2/NorpA at 4°C for 30 min, followed by centrifugation at 50,000 × g for 1 h. Pellets and supernatants were subsequently analyzed by Coomassie bright blue staining. Additionally, 1 mg/ml liposomes were incubated with a complex containing 3.26 μM EphB2 and varying concentrations (0, 1.63, 3.26 μM) of ephrin-A5 or ephrin-B2 in 100 μL of buffer (50 mM Tris–HCl [pH 7.5], 150 mM NaCl, 1 mM EDTA, and

1 mM DTT) at 4°C for 30 min. Following incubation, samples were centrifuged at 50,000 × g for 1 h, washed twice, and pellets and supernatants were subjected to Coomassie bright blue staining analysis.

QUANTIFICATION AND STATISTICAL ANALYSIS

All experiments were conducted independently in three independent replicates. Statistical analysis of the results was performed using GraphPad Prism (Software version 9.0). One-way ANOVA with Dunnett's post hoc test was used in evaluation of endogenous EphB2 or EphA4 phosphorylation level, and relative protein expression level in cultured cortical neurons. One-way ANOVA followed by Tukey's multiple comparisons test was used in the analysis of cell-based EphB2 kinase activation assay. Two-way ANOVA followed by Tukey's multiple comparisons test was used in the evaluation of ligand-induced receptor/ligand colocalization and HEK293T cell contraction. And an unpaired t-test was used to compared the relative expression level between EphB2 WT and EphB2 4Q. The Kd was determined by fitting a one-site-specific binding model of the binding reaction, and an R-squared value greater than 0.9. Dendritic complexity was evaluated by counting the number of intersections of dendrites with concentric circles centered on the soma using the Sholl analysis plugin in ImageJ software.[57] To quantitatively analyze dendritic spine density, we examined the number of dendritic spines from three representative dendritic segments per neuron. Data were presented as mean ± SD and statistical significance was set at $p < 0.05$. The statistical details of experiments were also presented in the figure legends.